Cardiac Microphysiological Devices with Flexible Thin-Film Sensors for Higher-Throughput Drug Screening

Supplementary Information

Johan U. Lind[1], Moran Yadid[1], Ian Perkins[1], Blakely B. O'Connor[1], Feyisayo Eweje[1], Christophe O. Chantre[1], Matthew A. Hemphill[1], Hongyan Yuan[1,2], Patrick H. Campbell[1], Joost J. Vlassak[3], Kevin K. Parker[1]*

[1] Disease Biophysics Group, John A. Paulson School of Engineering and Applied Sciences, Wyss Institute for Biologically Inspired Engineering, Harvard University, Cambridge, Massachusetts 02138, USA.

[2] Current Affiliations: Department of Mechanical, Industrial and Systems Engineering, University of Rhode Island, Kingston, RI, 02881 USA

[3] John A. Paulson School of Engineering and Applied Sciences, Harvard University, Cambridge, Massachusetts 02138, USA

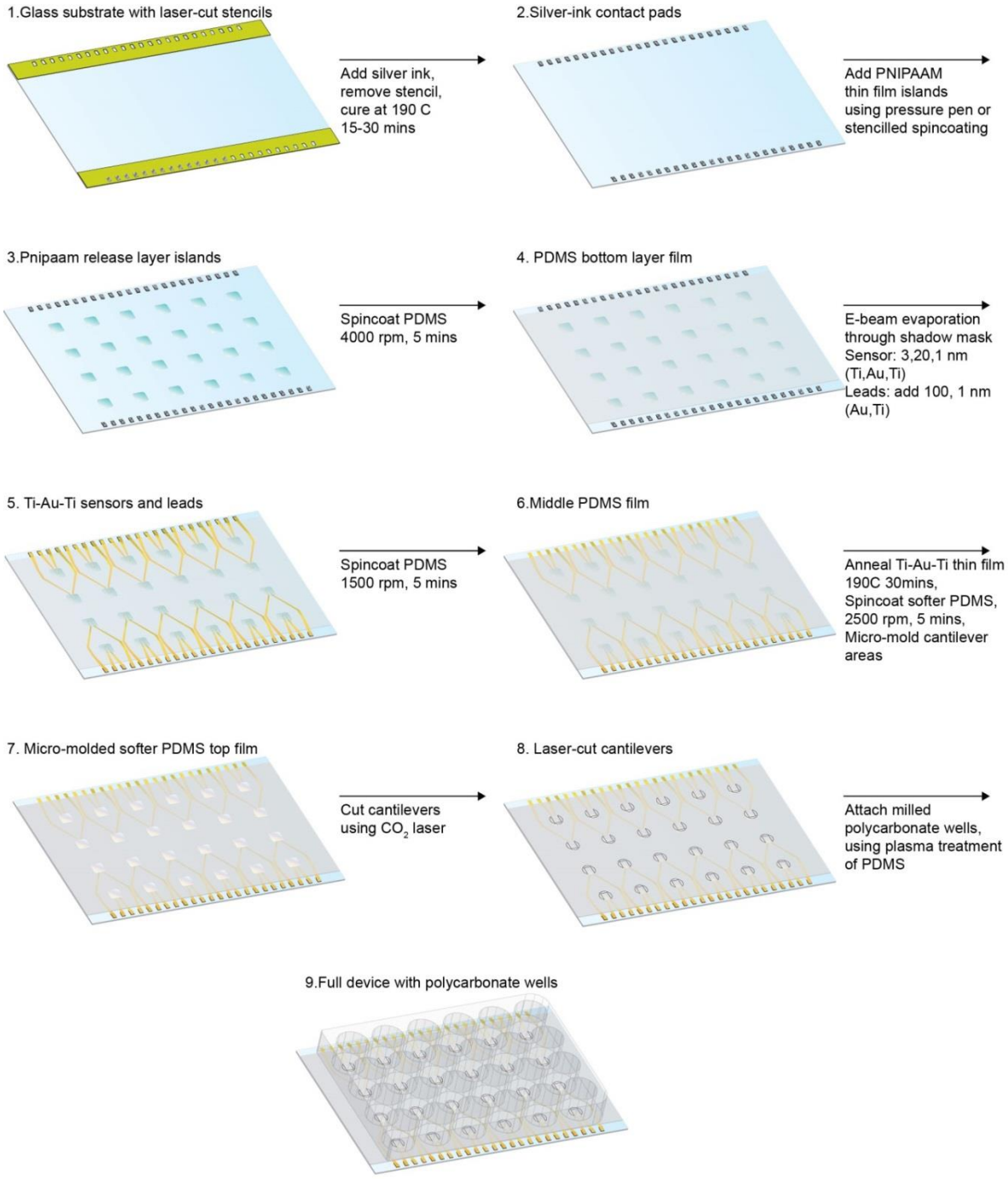

Supplementary Figure S1 | Device fabrication outline
Schematic illustration of the bottom-up fabrication procedure applied for the instrumented multi-well devices. See Methods & Materials section for details.

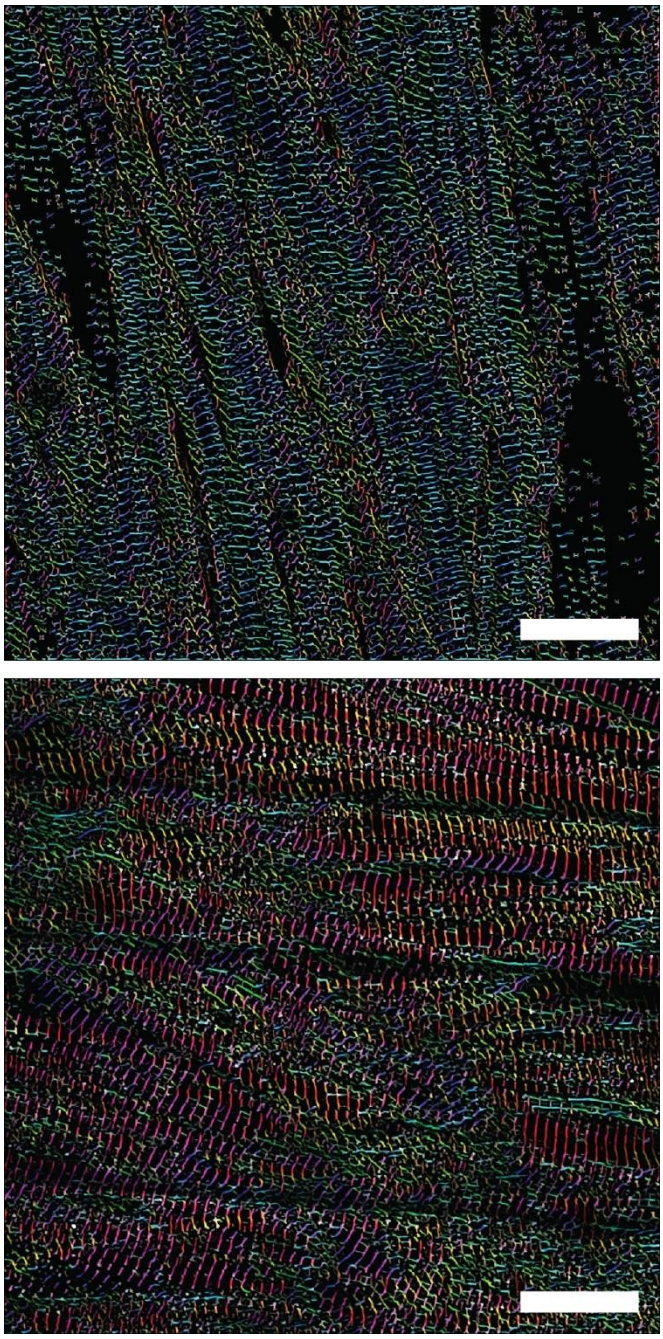

Supplementary Figure S2 | OOP anisotropy of engineered NRVM and hiPS-CM tissues.
Example confocal microscopy images processed for sarcomere OOP analysis. The angular orientation of α-actinin stained sarcomeres is indicated by color code. *Top:* NRVM tissue, with sarcomeres oriented horizontally, *Bottom:* hiPS-CM tissues, with sarcomeres oriented vertically. Scale bars: 20 µm. Average NRVM OOP: 0.4 (N=5), average hiPS-CM OOP: 0.31 (N=5).

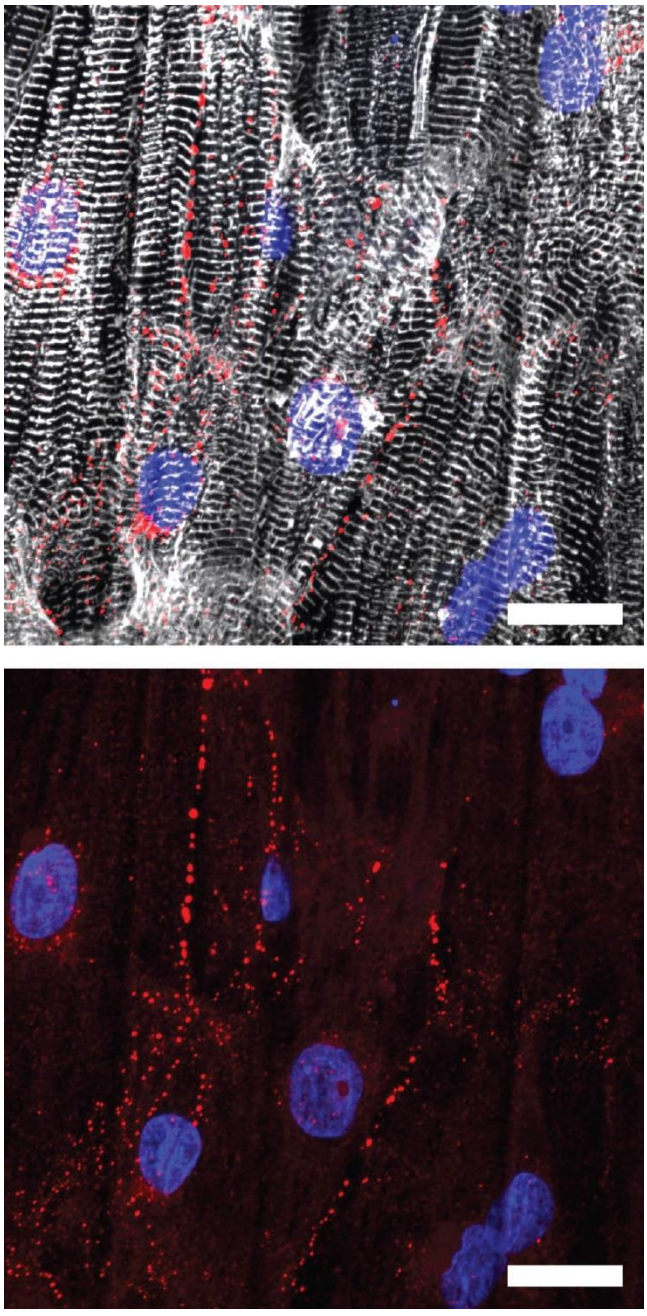

Supplementary Figure S3 | Engineered anisotropic hiPS-CM tissue
Confocal microscopy of immunostained hiPS-CM tissue on micro-molded PDMS (500 kPa) surface. Blue: DAPI nuclei stain, white: α-actinin, red: Cx43, Scale bars: 20 µm.

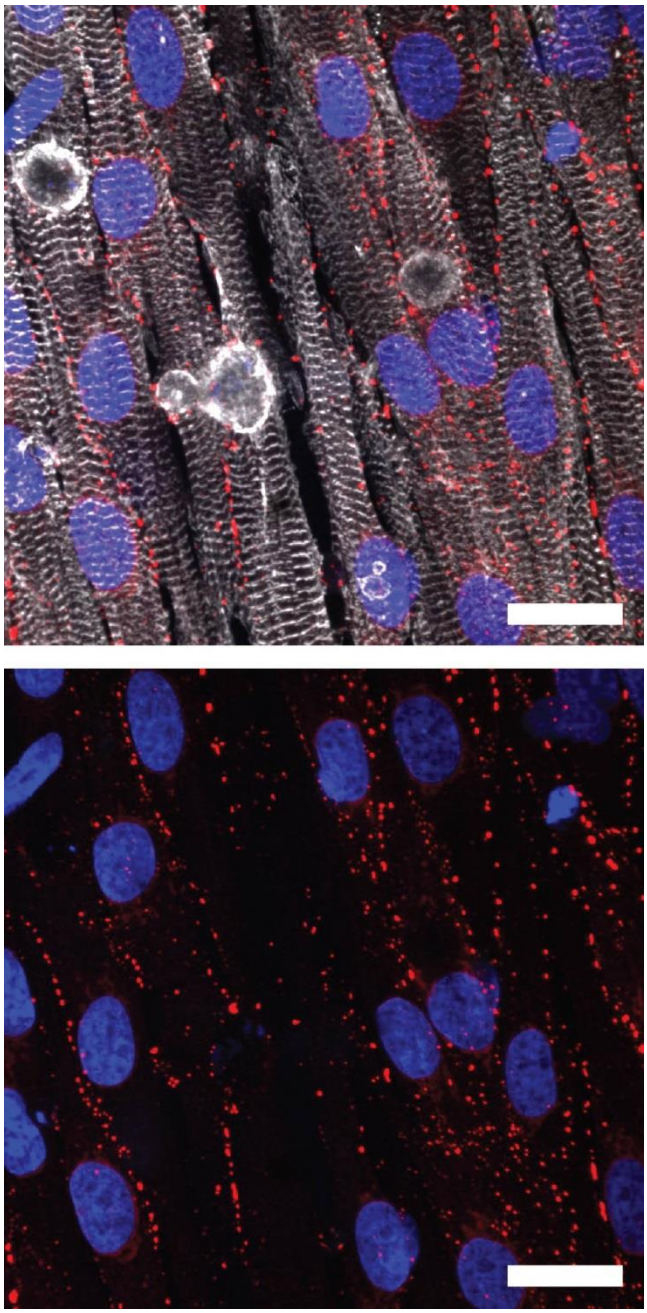

Supplementary Figure S4 | Engineered anisotropic NRVM tissue
Confocal microscopy of immunostained NRVM tissue on PDMS surface micro-contact printed with fibronectin. Blue: DAPI nuclei stain, white: α-actinin, red: Cx43, Scale bars: 20 µm. More pronounced electrical Cx43 connectivity seen for NRVM tissue, as compared to hiPS-CM tissue.

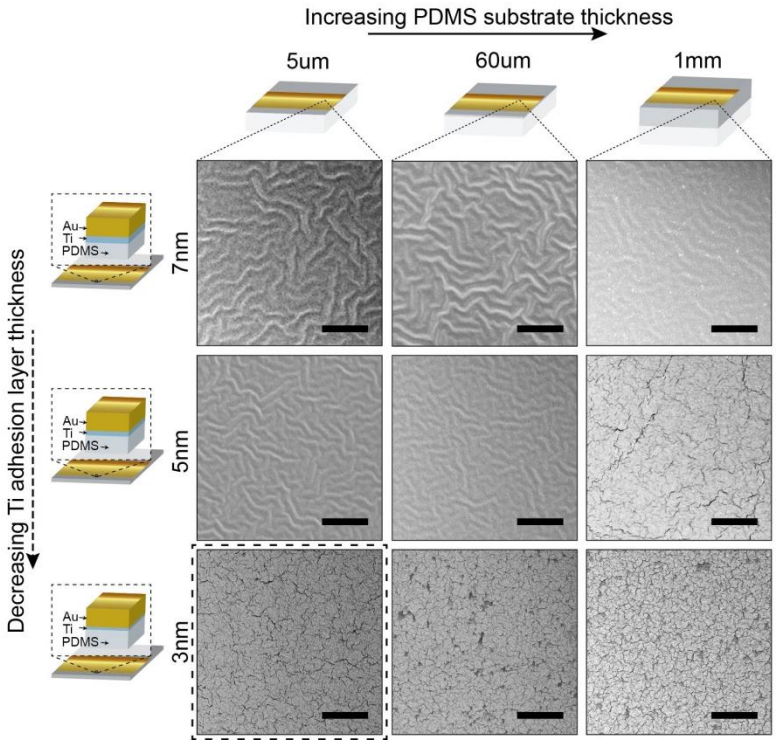

Supplementary Figure S5 | Titanium-Gold thin-film micro-structure is influenced by titanium adhesion layer thickness and PDMS substrate thickness. SEM images of Ti-Au-Ti thin films with layer thicknesses *X*-20-1 nm, deposited PDMS substrates with thicknesses ~5 µm, ~60 µm and ~1 mm. PDMS substrates were attached to glass supports. Scale bars 5 µm. Micro-buckled structures are induced by increasing Ti adhesion layer thicknesses and/or decreasing PDMS substrate thicknesses. Micro-cracks follow the opposite trend. Substrates were un-patterned surface with a ~1cm^2 area.

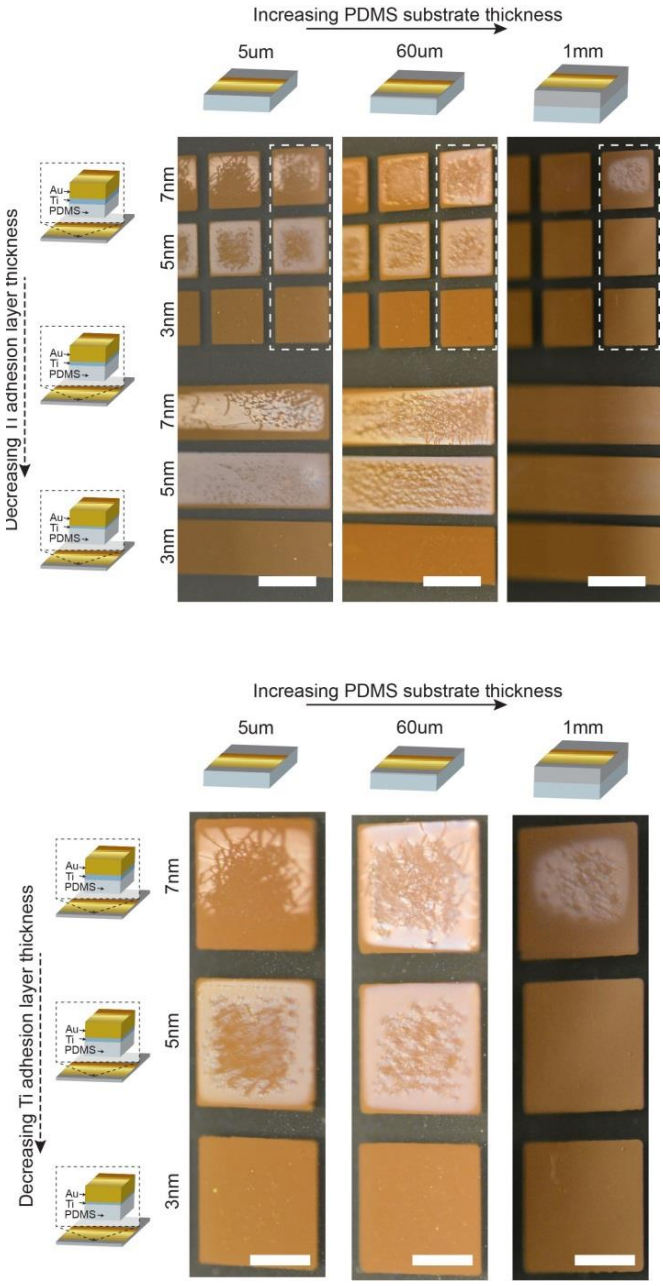

Supplementary Figure S6 | Titanium-Gold thin film appearance is influenced by PDMS substrate thickness and Ti adhesion layer thickness. Optical micrographs of Ti-Au-Ti thin films with layer thicknesses *X*-20-1 nm, deposited on PDMS substrates with thicknesses ~5 µm, ~60 µm and ~1 mm. PDMS substrates were attached to glass supports. Scale bars: *top*: 4 mm, *bottom:* 2 mm. Frosted refractive thin films are observed when increasing Ti adhesion layer thicknesses and/or decreasing PDMS substrate thicknesses. Frosting is most apparent in center of thin film islands, furthest from shadow mask edge. Frosted thin films

are micro-buckled in SEM and frequently display macroscopic failure cracks when patterned on the thin PDMS substrates.

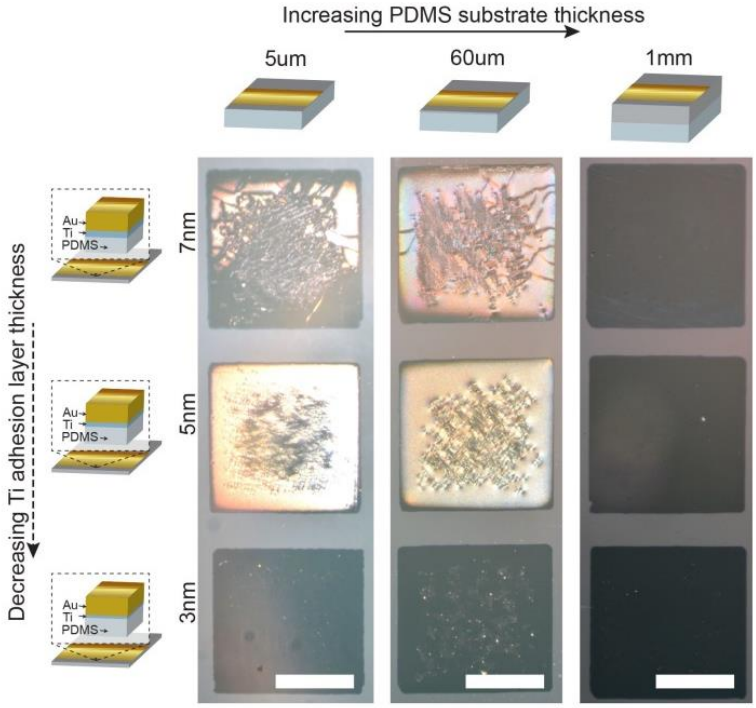

Supplementary Figure S7 | Titanium-Gold thin film appearance under significant backlight. Optical micrographs of Ti-Au-Ti thin films with layer thicknesses *X*-20-1 nm, deposited on PDMS substrates with thicknesses ~5 µm, ~60 µm and ~1 mm. PDMS substrates were attached to glass supports, and illuminated from back and partially from top. Scale bars: 2 mm. Bluish appearance observed for decreasing Ti adhesion layer thicknesses and/or increasing PDMS substrate thicknesses, and correlates with micro-cracking observed in the SEM.

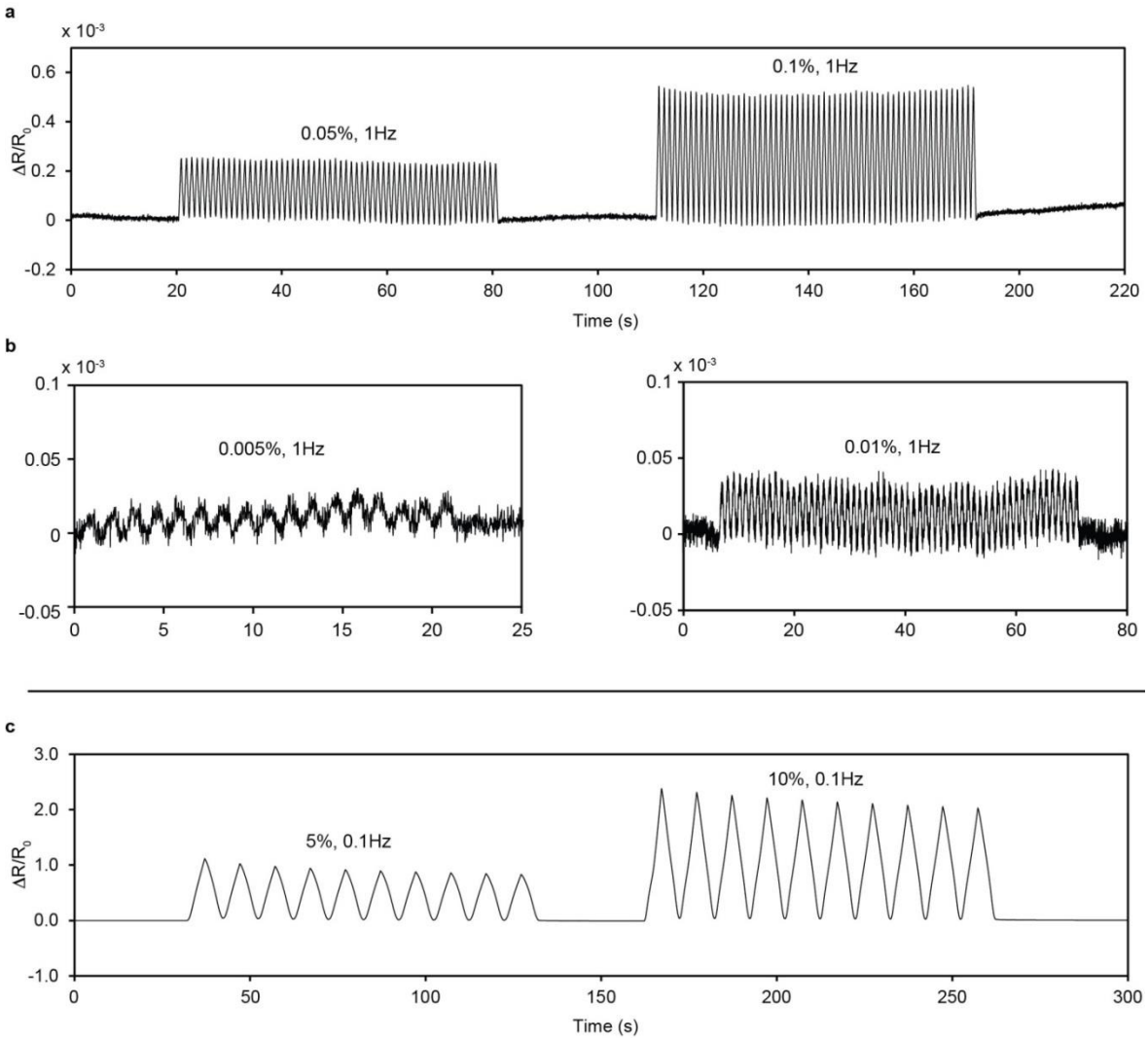

Supplementary Figure S8 | Strain tests of micro-cracked Ti-Au-Ti thin films

Relative change in resistance of 3,20,1 nm Ti-Au-Ti thin films deposited on 5 µm PDMS substrates, upon cyclic uniaxial strains. **(a)** 0.05 and 0.1 % strain, at 1 Hz **(b)** 0.005 and 0.01 % strain, at 1 Hz **(c)** 5 and 10 % strain at 0.1 Hz.

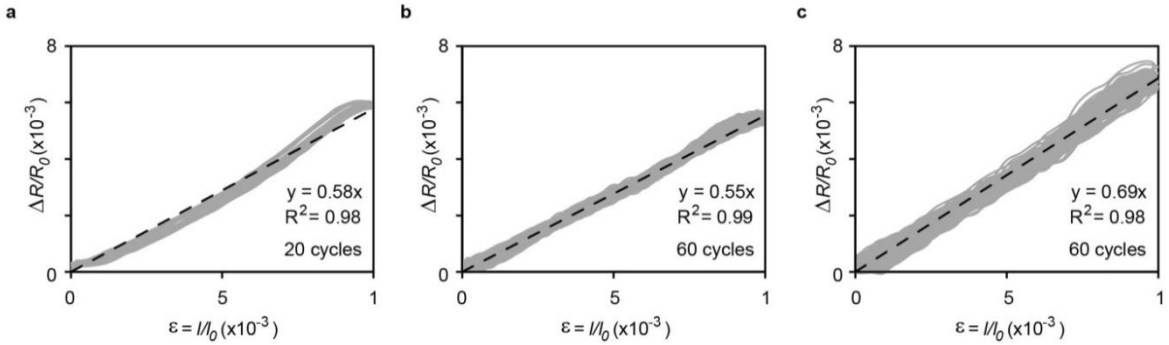

Supplementary Figure S9 | Micro-cracked thin-film gauge factor in 0.1% strain regime Relative resistance change of three separate 3, 20, 1 nm Ti-Au-Ti thin films deposited on 5µm PDMS substrates, upon cyclic uniaxial strain 0.1 % at 1 Hz. Relative resistance change thin films plotted vs. strain for 20 cycles. Linear fit (dashed line) indicate a gauge factor (GF) of app. 0.58 (a), 0.55 (b) and 0.69 (c) in the 0. 1% strain regime. Based on these tests, a GF value of 0.6 applied for conversion of device readouts.

General mechanical solution

The engineered muscle tissue is cultured on a rectangular cantilever. When the tissue contracts, a tension stress σ_{tissue} is generated within the tissue, and the cantilever substrate is bent to an arc with a radius of curvature R_{curv}, See Fig S10. Below, we derive a modified Stoney's equation describing the relationship between σ_{tissue}, the curvature, and the strain of each layer of the cantilever. This equation will serve to convert the electrical and optical measurements to the contractile stress of the tissue.

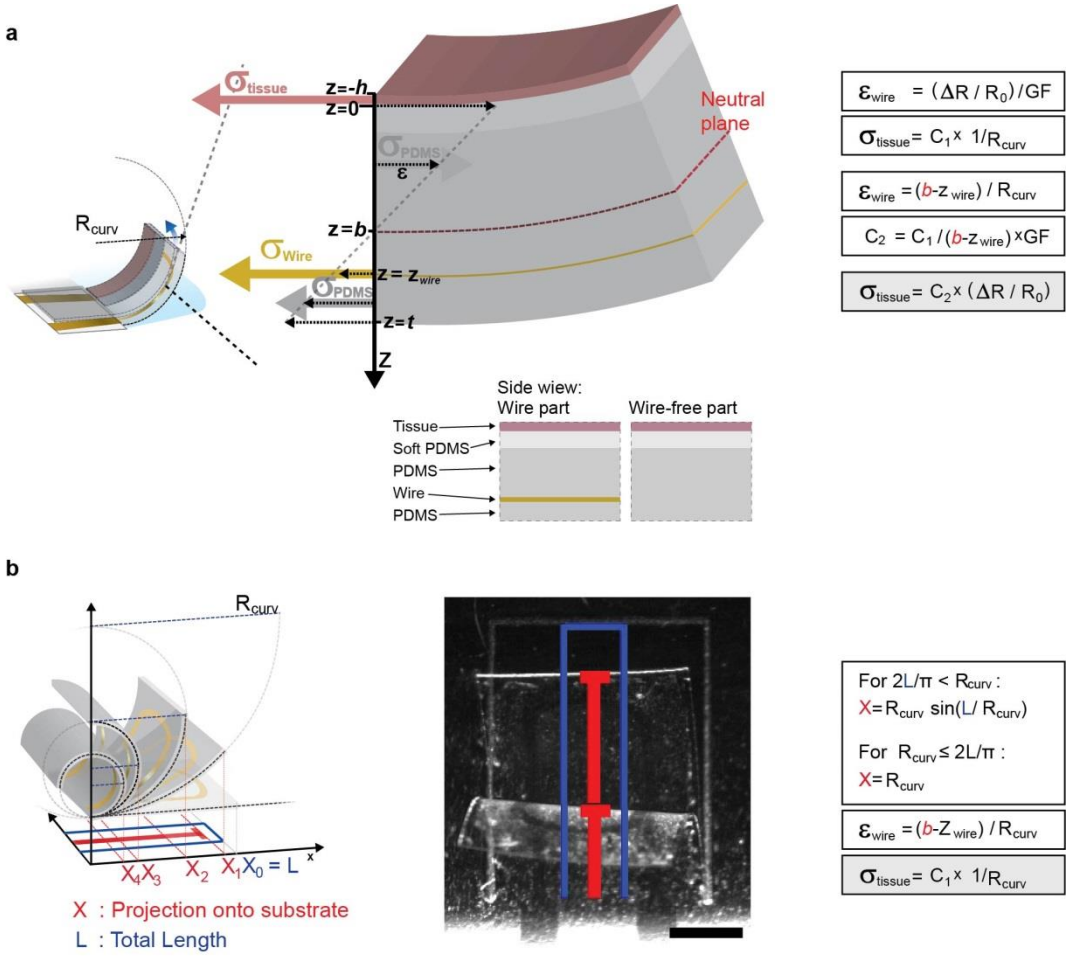

Figure S10 | (a) Free body diagram of an elementary strip of the cantilever, indicating placement of neutral plane *b* relative to strain gauge wire and the linear relationship between relative resistance change and tissue stress of the applied model **(b)** Optical tracking of cantilever radius of curvature, and linear relationship between curvature of the applied model. Conversion constants C_1 and C_2, were determined through mechanical and geometric characterization of the cantilever layers.

Variables in the modified Stoney's equation	
σ_{tissue}	Stress (tension) in the cell layer
h	Thickness of the cell layer
R_{curv}	Radius of curvature cantilever
t	Thickness of layer of cantilever
E	Young's modulus of layer of cantilever
v	Poisson's ratio of layer of cantilever
ε_x	Strain in the cantilever layer
σ_x	Normal stress in the cantilever layer
b	Distance between neutral surface of bending and the tissue-cantilever interface
W	Width of the cantilever

Supplementary Table S1 | Notation applied for variables in modified Stoney's equation mechanical model

Following the methodology of Stoney, we ignore the bending resistance of the tissue film itself (Stoney, G., *The Tension of Metallic Films Deposited by Electrolysis*, Proc. R. Soc. Lond. A May 6, 1909 82 553 172-175). This approximation is grounded in the fact that the tissue is orders of magnitudes more compliant than the substrate layers (10kPa <1MPa). However, due to the non-negligible thickness of the tissue, the tissue thickness will be taken into account when calculating the active bending moment.

The instrumented cantilever has a width-to-thickness ratio of ~100 and consists of two distinct strips: a thin-film sensor-containing strip and the wire-free strip. Given the large width-to-thickness ratio and the low stiffness of the cantilever materials, we assume that the two regions have different neutral surfaces, and ignore the any transition zones between these distinct regions. To make the model mathematically tractable, we further assume that the two strips have the same numerical radius of curvature relative to the separate neutral surfaces, when subjected to tissue contraction. For each strip, cylindrical bending theory will be applied to solve for the position of the neutral surface to yield a final modified Stoney's equation. In the derivation, we focus on the static equilibrium of an elementary strip cut through a plane perpendicular to the cantilever length, and a small distance from the free end, see Fig S10. All the boundaries of this free body, other than the cut surface, are free boundaries. Due to the static equilibrium of the free body, the sum of normal forces and the sum of the moments on the cut surface must equal zero:

$$\int_0^t \sigma_x W dz + \sigma_{tissue} h W = 0 \Leftrightarrow \int_0^t \sigma_x dz + \sigma_{tissue} h = 0 \qquad \textbf{(1)}$$

$$\int_0^t \sigma_x z W dz - \sigma_{tissue} h W \frac{h}{2} = 0 \Leftrightarrow \int_0^t \sigma_x z dz - \sigma_{tissue} h \frac{h}{2} = 0 \qquad \textbf{(2)}$$

Let b denote the distance from the bottom of the tissue to the neutral surface. The normal strain ε_x in the longitudinal direction can then be written as:

$$\varepsilon_x(z) = \frac{b-z}{R_{curv}} \qquad \textbf{(3)}$$

The wire-containing strip of the cantilever is composed of 4 layers: PDMS layer 1, Gold thin film, PDMS layer 2, Soft PDMS top layer. The normal stress distribution $\sigma_x(z)$ in each layer can be obtained from an extended beam theory. Given the anisotropic nature of the tissue and uniaxial contraction, we can further assume cylindrical curvature and uniform strain in the width direction. Finally, due to the large width to thickness ratio, the cantilever will be treated as a plate. (Timoshenko, S. and Woinowsky-Krieger, S., *Theory of plates and shells*. 2d ed. Engineering societies monographs, 1959: McGraw-Hill). The normal stress σ_x for the i-th layer is then:

$$\sigma_x^i = \frac{E_i}{1-v_i^2}\varepsilon_x = \frac{E_i}{1-v_i^2}\frac{(b-z)}{R_{curv}} \qquad \textbf{(4)}$$

Substituting equation (4) into equation (1) we obtain:

$$b = \frac{B}{C} + \frac{R_{curv}\sigma_{tissue}h}{C} \qquad \textbf{(5)}$$

where $B = \sum_{i=1}^{n=no\ of\ layers} \frac{E_i}{1-v_i^2}\frac{1}{2}\left({z_{top}^i}^2 - {z_{bottom}^i}^2\right)$,

and $C = \sum_{i=1}^{n=no\ of\ layers} \frac{E_i}{1-v_i^2}\left(z_{top}^i - z_{bottom}^i\right)$.

Similarly substituting equation (4) into equation (2) we obtain:

$$b = \frac{A}{B} - \frac{R_{curv}\sigma_{tissue}}{B}\frac{h^2}{2} \qquad \textbf{(6)}$$

where $A = \sum_{i=1}^{n=no\ of\ layers} \frac{E_i}{1-v_i^2}\frac{1}{3}\left({z_{top}^i}^3 - {z_{bottom}^i}^3\right)$

The tissue stress can now be derived by equating (5) and (6):

$$\sigma_{tissue} = \frac{1}{R_{curv}} \cdot \frac{\left(\frac{AC}{B} - B\right)}{\left(\frac{h^2C}{2B} + h\right)} \qquad \textbf{(7)}$$

Similarly, the neutral axis placement can be obtained:

$$b = \frac{2A+hB}{2B+hC} \qquad \textbf{(8)}$$

This solution holds for the wire-containing part of the cantilever. For the wire-free strip, the same procedure can be taken to derive the position of the neutral surface $\hat{b}$ from (8), as well as the relationship between the curvature c and the contractile stress $\hat{\sigma}_c$ in the wire-free strip from (7).

To obtain an equivalent collected tissue stress, we assume that the stress is uniform across the width of the tissue. Such a collected contractile stress σ_c is then equivalent to the geometric average of the apparent contractile stresses in the wire-containing strip and the wire-free strip,

$$\sigma_c = \frac{\sigma_c W + \hat{\sigma}_c \hat{W}}{W + \hat{W}} \qquad \textbf{(9)}$$

where $\hat{W}$ and W are the widths of the wire-free and wire-containing strips, respectively. Assuming a constant gauge factor, the electrical readout can be converted to cantilever curvature using:

$$\frac{z_{wire} - b}{R_{curv}} \cdot GF = \frac{R - R_0}{R_0} \qquad \textbf{(10)}$$

$$\frac{1}{R_{curv}} = \frac{1}{GF(z_{wire} - b)} \frac{R - R_0}{R_0} \qquad \textbf{(10.1)}$$

This allowing stresses to be directly obtained from gauge readout applying (7) and (9)

Calibration and determining effective Young's modulus of microcracked gold thin film

By performing mechanical tests and thickness profiling for each layer, we determined the thickness and Young's modulus of each PDMS based layer in the cantilever, Table S2. Note ν = 0.5 is assumed for all layers.

	Young's modulus, *E*
PDMS reg. cure	1.61 Mpa
PDMS 190°C anneal	1.99 Mpa
Soft PDMS composition	548 kPa
Ti-Au-Ti micro-cracked film	0.787 GPa

	Layer thicknesses *t*
Bottom PDMS (5000 rpm)	3.3 µm
Bottom PDMS (4000 rpm)	5.2 µm
Ti-Au-Ti film	20 nm
Middle PDMS (2000 rpm)	11.9 µm
Middle PDMS (1500 rpm)	16.2 µm
Soft PDMS top (2500 rpm)	6.2 µm

Supplementary Table S2 | Experimentally determined constants applied in mechanical model. For all PDMS layers values represent average values (N=3). For the thin-film layer, a nominal thickness of 20 nm was assumed, while the effective Young's modulus was determined based on optical tracking of cantilevers. Poisson's ratio of 0.5 was assumed for all layers.

However, the effective Young's Modulus of the micro-cracked gold thin film cannot be determined using bulk measurements; this also means that the placement of the neutral plane cannot be determined. Instead, we determine these experimentally by comparing concurrent optical and electrical tracking cantilever movements. It follows from (10.1) that there is a linear relationship between the curvature and resistance of the gauge:

$$\frac{1}{R_{curv}} \cdot (z_{wire} - b) \cdot GF \cdot R_0 + R_0 = R \quad \textbf{(10.2)}$$

By using concurrent recordings of curvature and resistance, and applying GF = 0.6 as determined above for the relevant strain regime of 0.1%, we can obtain $(z_{wire} - b)$ and thus b.

Rewriting A, B and C, we then get:

$$A = A^{no\ wire} + E_{wire}^{eff} \frac{1}{3} ({z_{topwire}}^3 - {z_{bottomwire}}^3)$$

$$B = B^{no\ wire} + E_{wire}^{eff} \frac{1}{2} ({z_{topwire}}^2 - {z_{bottomwire}}^2)$$

$$C = C^{no\ wire} + E_{wire}^{eff} (z_{topwire} - z_{bottomwire})$$

Inserting the reformulated expressions for A, B and C into **(8)**, we get E_{wire}^{eff} as a function of the experimental value of b:

$$E_{wire}^{eff} = \frac{-bhC^{no\ wire} - (2b-h)B^{no\ wire} + 2A^{no\ wire}}{\left(bh(z_{topwire} - z_{bottomwire}) + \left(b - \frac{h}{2}\right)({z_{topwire}}^2 - {z_{bottomwire}}^2) - \frac{2}{3}({z_{topwire}}^3 - {z_{bottomwire}}^3)\right)} \quad \textbf{(11)}$$

After determining the effective Young's modulus of the micro-crack gold wire the system is fully described and the conversion constant from resistance and curvature to tissue stress, can be calculated from cantilever geometry following (8) and (10.1).

Calculating relative changes in twitch stress

We applied a localized baseline value for calculating relative changes in active stresses, such as twitch stress, from the electrical readout. This is grounded in the following approximation:

$$\Delta\sigma_{tissue} = constant \cdot \frac{1}{R_0}\left(R_{sys} - R_{dia}\right) \sim constant \cdot \frac{1}{R_{dia}}\left(R_{sys} - R_{dia}\right) \quad \textbf{(12)}$$

Based on the optical calibrations, this approximation introduces an error of less than 1%. Further, drift in R_{dia} baseline value observed during recordings of several minutes to hours, were found to in the order of 0.01-0.1% compared to R_0, and thus of negligible influence on twitch stress values.

We note that the model is static in nature and does not take viscous effects into account. This leads a relative underestimation of twitch stress values for higher frequencies, as compared to lower frequencies where these effects are less pronounced. This could in part explain the negative force-frequency relationships observed for both NRVM and hiPS-CM thin film tissues. (Bahador, M., Yuan H., *The effect of viscous force on the prediction of muscle contractility in biohybrid cantilever-based experiments*. Extreme Mechanics Letters 9 (2016): 342-346).

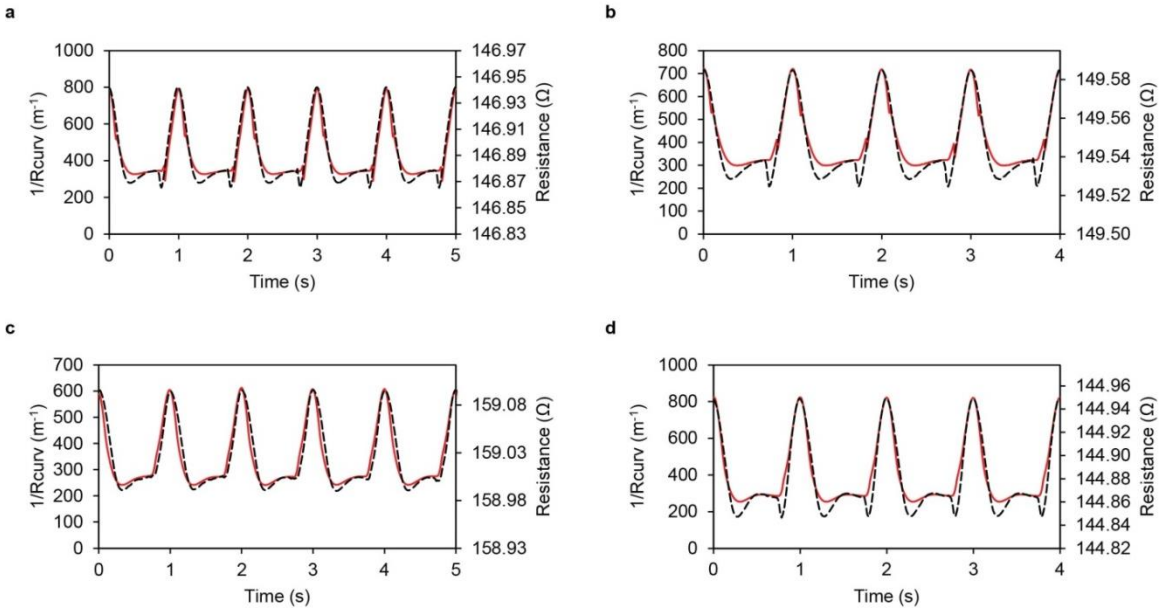

Figure S11 | Concurrent optical tracking of curvature (red, right axis) and electrical readout or resistance (dashed black, right axis) from four independent cantilevers

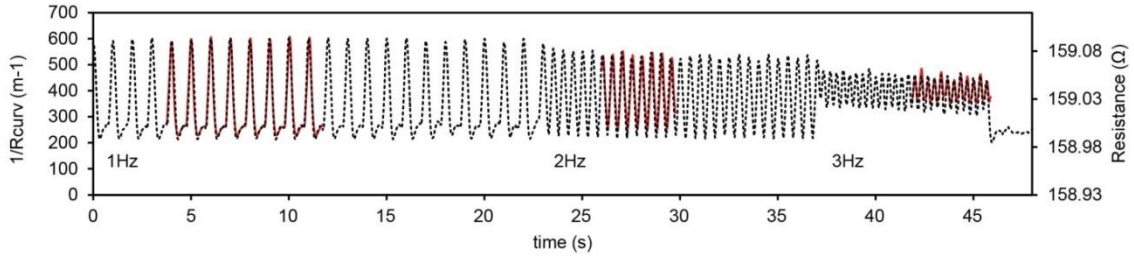

Figure S12 | Concurrent optical tracking of curvature and electrical readout of resistance at a range of pacing frequencies.

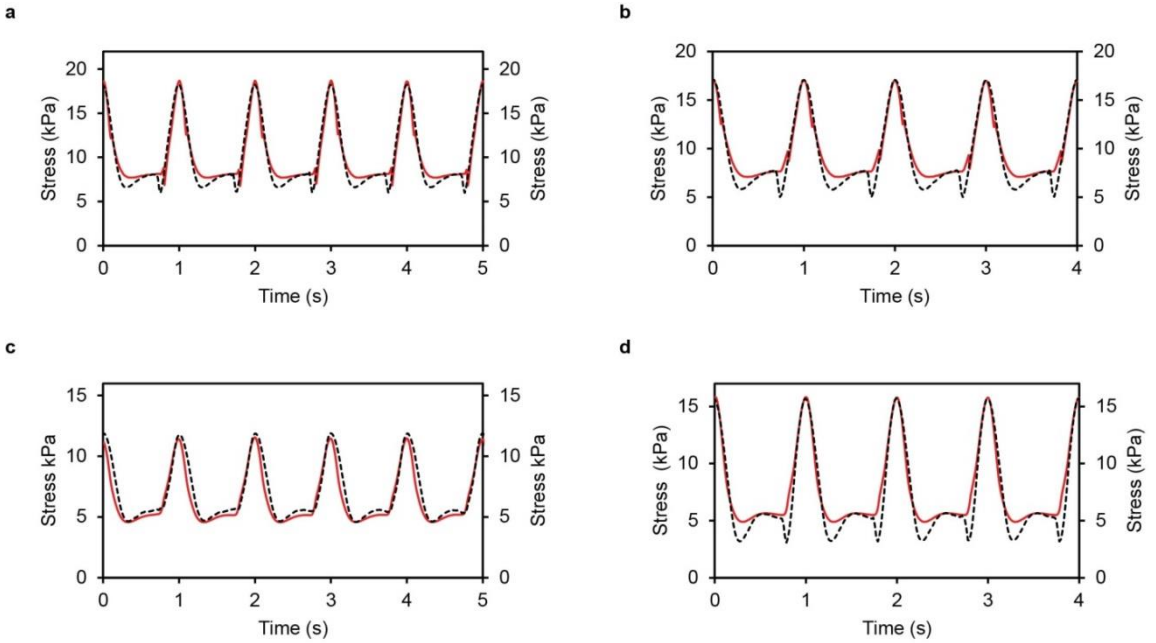

Figure S13 | Stress values from optical tracking data (red, right axis) and electrical readout (dashed black, right axis) from four independent cantilevers, using effective gold stiffness calculated from specific cantilever through optical tracking.

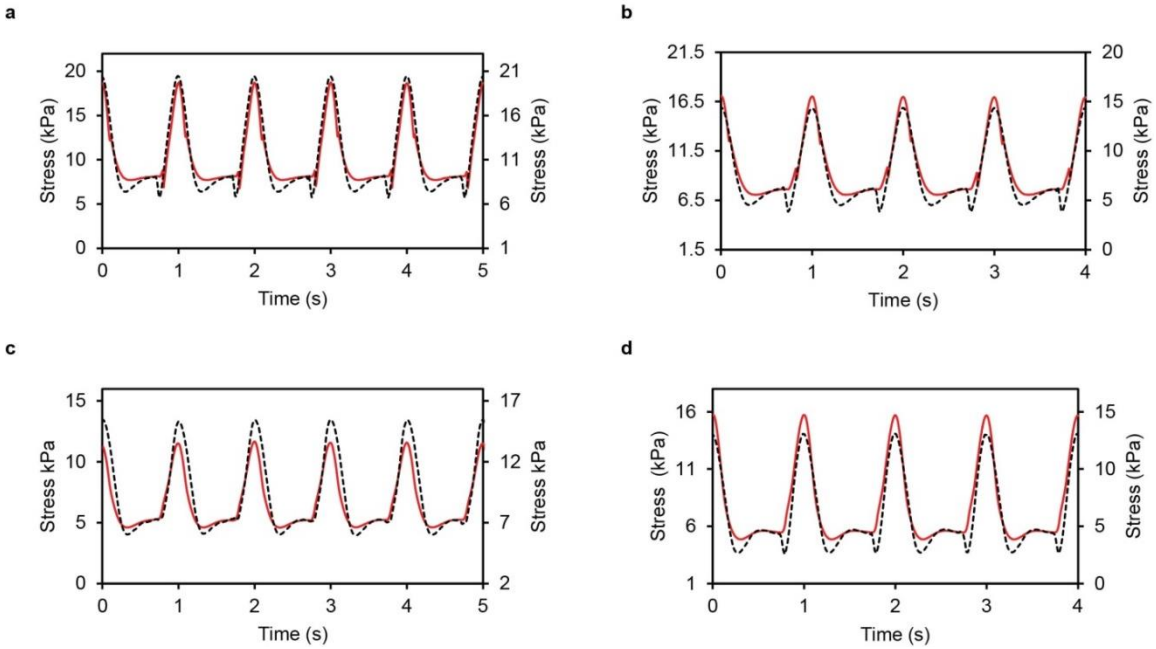

Figure S14 | Stress values from optical tracking data (red, right axis) and electrical readout (dashed black, right axis) from four independent cantilevers, using average effective gold thin film Young's modulus of 0.787 GPa for all samples.

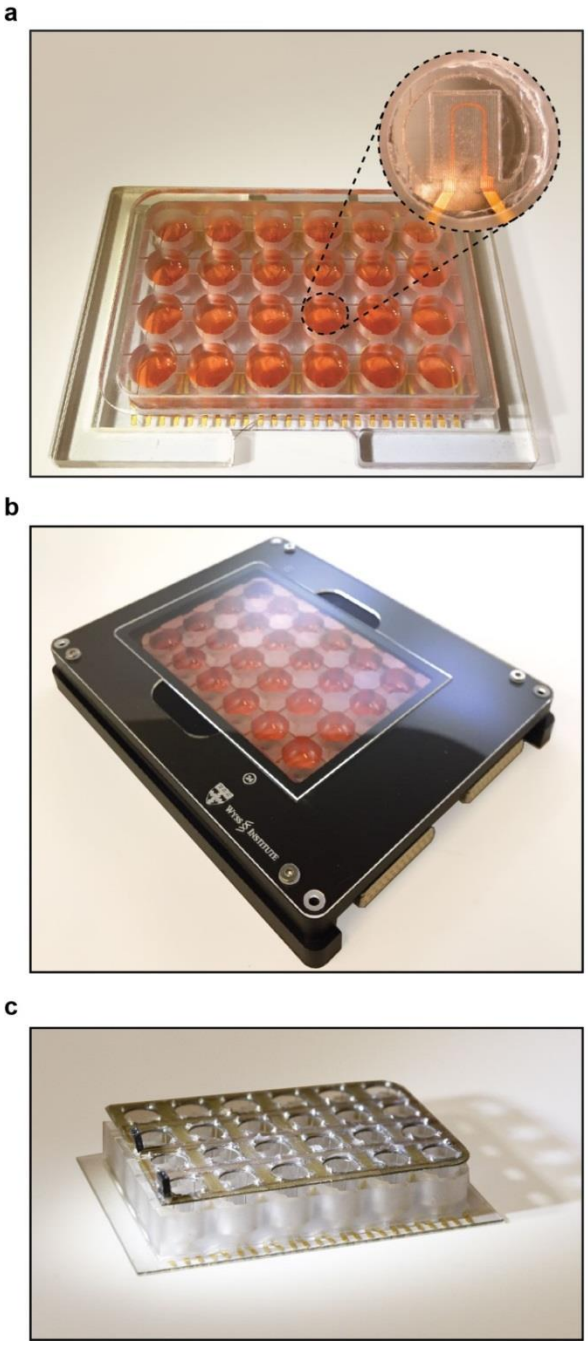

Figure S15 | 24-Well device (a) Instrumented 24-well device filled with cell media. *Insert:* Example cantilever in well. **(b)** Custom recording setup applied for in-incubator recordings. **(c)** Custom pacing insert for electrically pacing tissue contraction. Pacing wires are based on platinum.

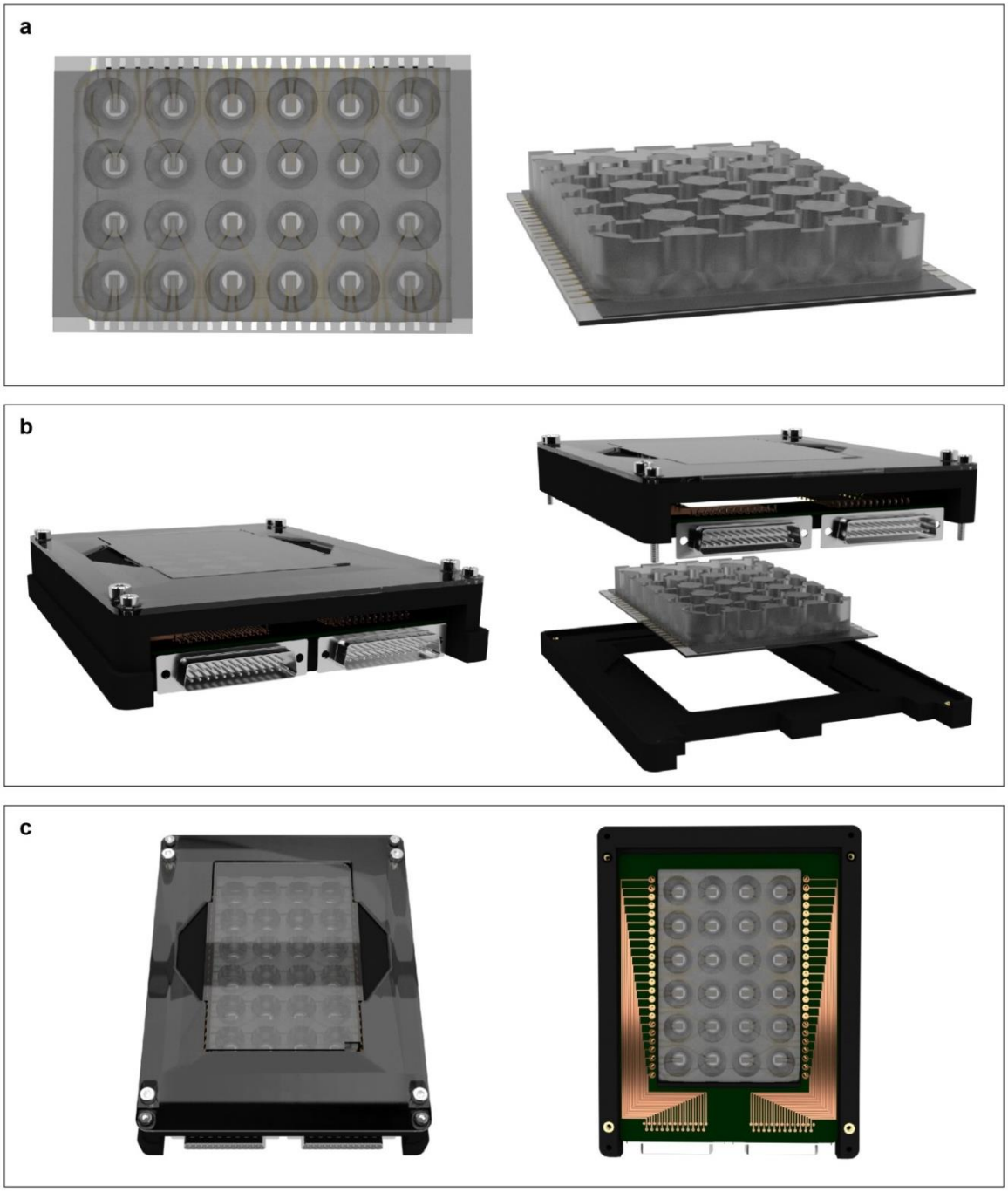

Figure S16 | 24-Well device design (a) Rendering of 24-well device **(b)** Rendering of device in recording holder, showing assembly and disassembly process **(c)** Interior of top part of recording holder with embedded PCB wiring.

Figure S17 | 8-Well device prototype applied in initial tests and NRVM-based experiments.

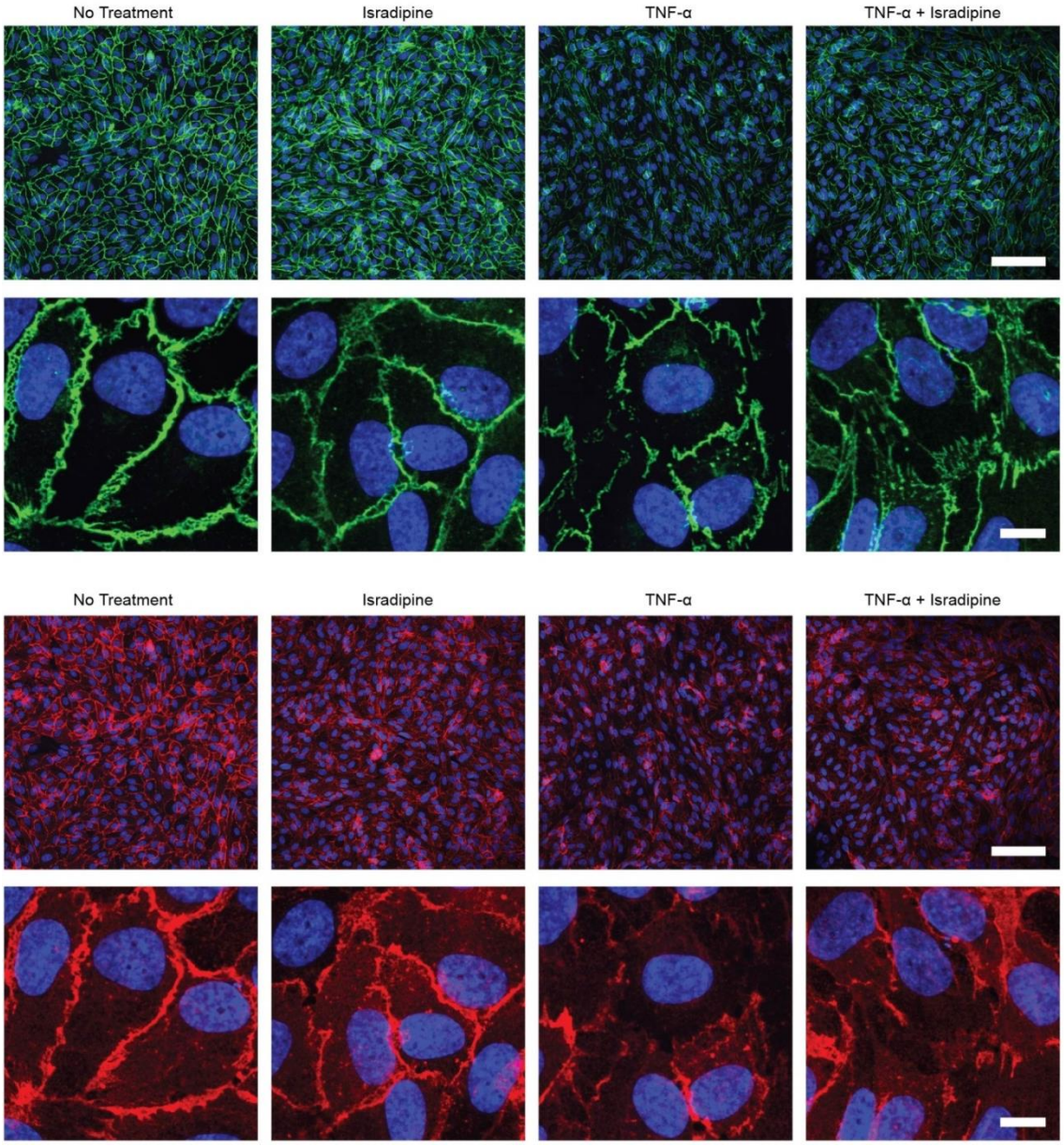

Figure S18 | Endothelial barrier perturbation. Confocal microscopy of immunostained unperturbed HUVEC endothelial barriers in Transwell® substrates, and barriers after 6 h exposure to 100 nM Israpidine, 20 ng/ml TNF-α and 100 nM Israpidine + 20 ng/ml TNF-α. Blue: DAPI nuclei stain, green: VE-Cadherin, red: PECAM. Scale bars row 1 and 3: 100 µm, row 2 and 4: 10 µm

Supplementary Movie 1| Spontaneously beating instrumented cantilever. Tissue based on NRVM, recorded at day 4 after seeding.